Han WANG, Mingjie PANG, Hai LIN, 2022. Enhanced solution to the surface–volume–surface EFIE for arbitrary metal–dielectric composite objects. *Frontiers of Information Technology & Electronic Engineering*, 23(7):1098-1109. https://doi.org/10.1631/FITEE.2100387

Enhanced solution to the surface–volume–surface EFIE for arbitrary metal–dielectric composite objects

Key words: Composite object; Integral equation; Method of moments (MoM); Addition theorem; Iterative method

Corresponding author: Hai LIN
E-mail: lin@cad.zju.edu.cn
ORCID: https://orcid.org/0000-0002-1682-8465

Motivation

1. To simulate the scattering properties of metal–dielectric objects, the surface–volume–surface electric field integral equation (SVS-EFIE) has been proposed in previous works.

2. SVS-EFIE can lead to complex equations, laborious implementation, and unacceptable computational complexity in the method of moments (MoM).

3. A more general formulation of SVS-EFIE is required.

4. The addition theorem and iterative method can help improve the efficiency.

Main idea

1. A general matrix equation (GME) is presented to solve the SVS-EFIE using MoM for composite metal–dielectric composite objects consisting of any number of sub-regions.

2. Two acceleration policies are proposed to solve GME based on the coupling degree, which can be set adaptively to balance the accuracy and efficiency.

Method

The GME for arbitrary metal–dielectric composite objects can be written as

$$V^p = \begin{cases} \sum_{q=1}^{P_c} Z_{SS}^{pq} I^q - \sum_{q=P_c+1}^{P_c+P_d} Z_{SVS}^{pq} I^q, \; p \in [1, P_c], \\ Z_{SS}^{p} I^p - \sum_{q=1}^{P_c} Z_{SS}^{pq} I^q - \sum_{q=P_c+1}^{P_c+P_d} Z_{SVS}^{pq} I^q, \\ \quad p \in [P_c + 1, P_c + P_d]. \end{cases} \tag{12}$$

Method

For the strong coupling case, the addition theorem is adopted to accelerate matrix-vector-multiplication (MVM).

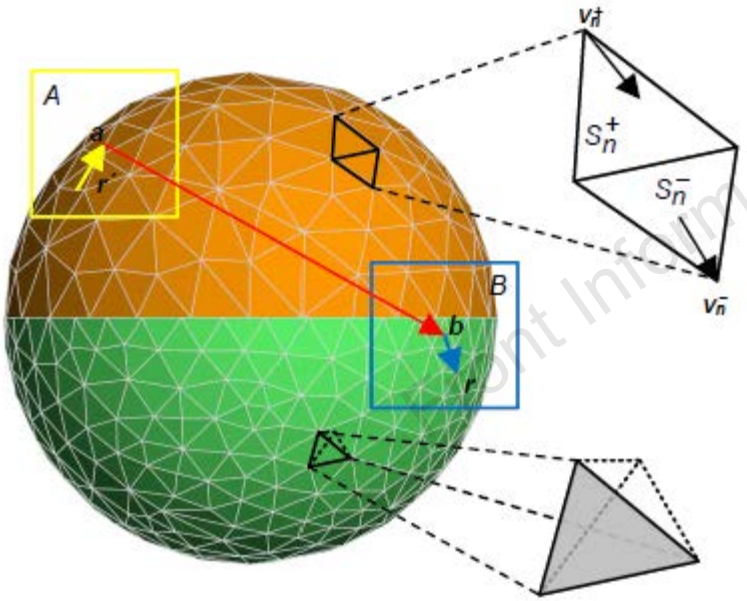

$$\overline{\overline{G}}_{\mathrm{e}0,\mathrm{e}\epsilon_q}(\boldsymbol{r},\boldsymbol{r}') = \left(\overline{\overline{I}} - \frac{\nabla\nabla'}{k_{0,\epsilon_q}^2}\right)\frac{\mathrm{e}^{-\mathrm{i}k_{0,\epsilon_q}|\boldsymbol{r}-\boldsymbol{r}'|}}{4\pi|\boldsymbol{r}-\boldsymbol{r}'|}$$

$$= \frac{1}{4\pi}\int\left(\overline{\overline{I}} - \hat{\boldsymbol{k}}\hat{\boldsymbol{k}}\right)\mathrm{e}^{-\mathrm{i}k_{0,\epsilon_q}\hat{\boldsymbol{k}}(\boldsymbol{r_{rb}}-\boldsymbol{r_{r'a}})} \cdot T_L(k_{0,\epsilon_q},\hat{\boldsymbol{k}},\boldsymbol{r_{ba}})\mathrm{d}^2\hat{\boldsymbol{k}},\ |\boldsymbol{r_{ba}}| < |\boldsymbol{r_{rb}}| + |\boldsymbol{r_{r'a}}|, \tag{20}$$

$$T_L(k_{0,\epsilon_q},\hat{\boldsymbol{k}},\boldsymbol{r_{ba}}) = \frac{k}{4\pi}\sum_{l=0}^{L}(-\mathrm{i})^{l+1}(2l+1)h_l^{(2)}(k_{0,\epsilon_q}|\boldsymbol{r_{ba}}|)P_l(\hat{\boldsymbol{k}}\hat{\boldsymbol{r}}_{\boldsymbol{ba}}), \tag{21}$$

$$\begin{aligned}\boldsymbol{r}-\boldsymbol{r}' &= (\boldsymbol{r}-\boldsymbol{b}) + (\boldsymbol{b}-\boldsymbol{a}) - (\boldsymbol{r}'-\boldsymbol{a}) \\ &= \boldsymbol{r_{rb}} + \boldsymbol{r_{ba}} - \boldsymbol{r_{r'a}}.\end{aligned} \tag{22}$$

Method

For the weak coupling case, the iterative method and adaptive cross are adopted.

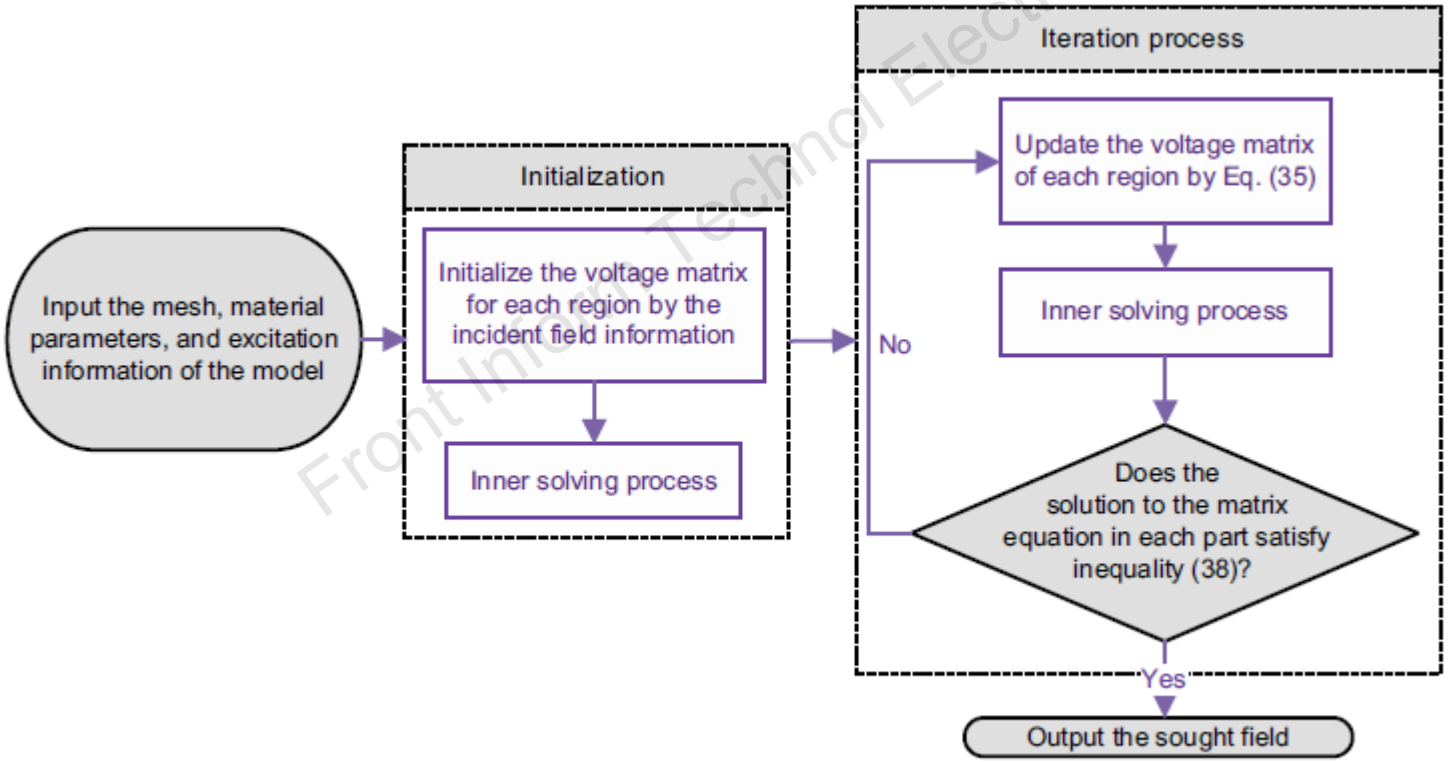

Fig. 2 General flowchart of the enhanced solution in the weak coupling case

Major results

Table 1 Computational resource requirements of the direct and enhanced solutions

Model	N_s	N_v	Time (s)		Decrease in time (%)	Memory (MB)		Decrease in memory (%)	Iteration
			Direct	Enhanced		Direct	Enhanced		
Almond	3753	10 911	839.20	188.40	77.60	6128.70	1106.70	81.94	77
Stratified ball	10 833	31 652	3370.88	352.04	89.60	24 479.00	2705.11	88.90	80
Composite ball	21 915	72 299	45 234.50	1546.30	96.60	64 879.20	6490.33	90.00	138
Discrete object	15 404	74 423	14 008.70	1446.43	89.70	64 021.60	5143.57	92.00	79

N_s: number of triangle pairs; N_v: number of tetrahedrons; Iteration: number of iteration steps in the enhanced solution

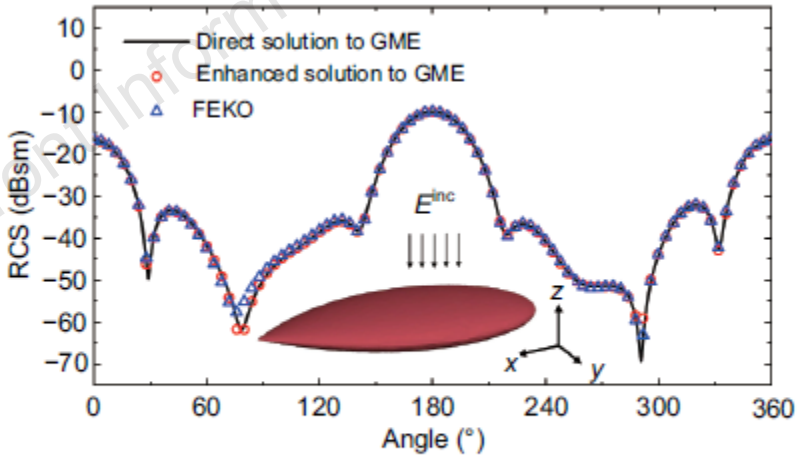

Fig. 3 Bistatic RCS of the almond computed by the direct solution, enhanced solution, and FEKO

Major results

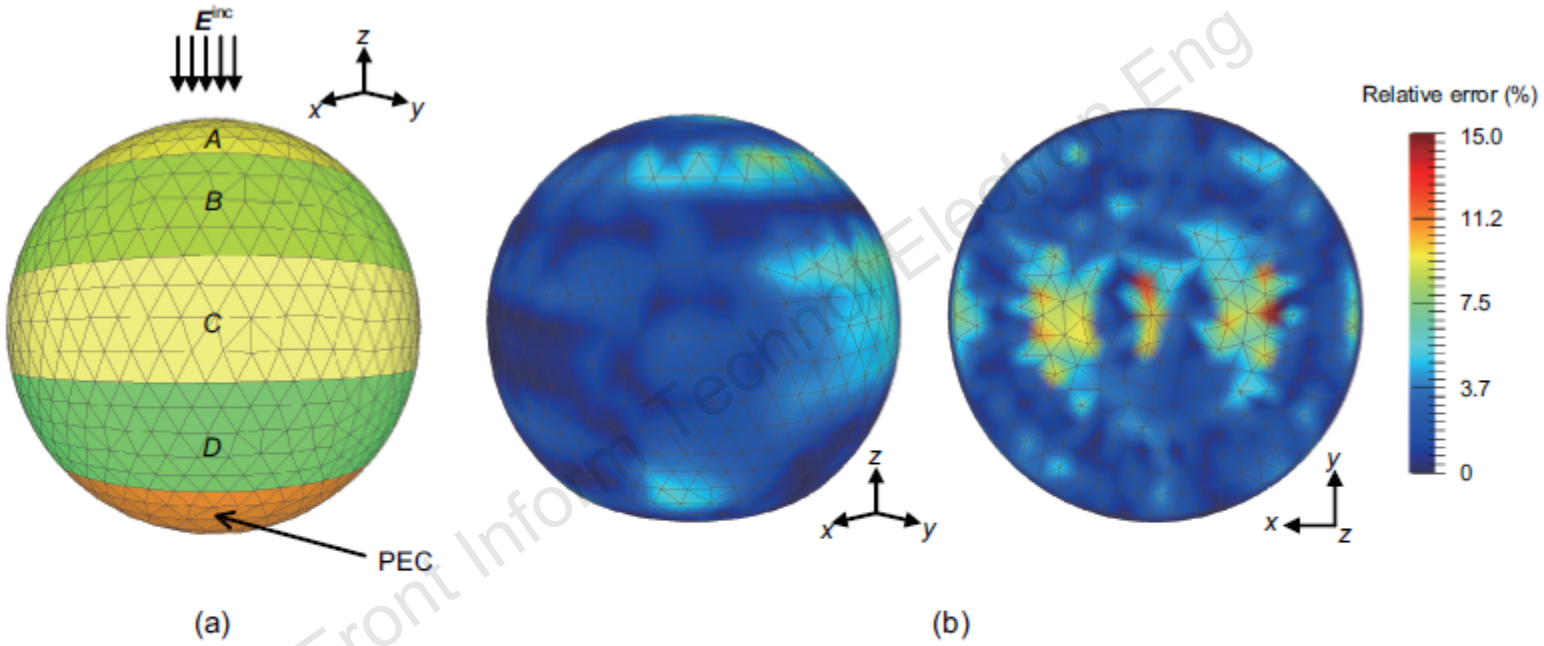

Fig. 4 Model and simulation results of the stratified ball

(a) The ball centered at the origin consists of five sub-regions with the same thickness of 0.04 m. The sub-region at the bottom of the ball is formed by PEC, and the other sub-regions are formed by dielectric materials A, B, C, and D with relative permittivity of 1.5, 2.0, 2.5, and 3.0, respectively. The stratified ball is illuminated by a 1.5 GHz vertically polarized incident wave from $(\theta, \phi) = (0°, 0°)$. (b) The relative error distribution among the dielectric sub-regions of the enhanced solution with respect to the FEKO solution is represented by different colors

Major results

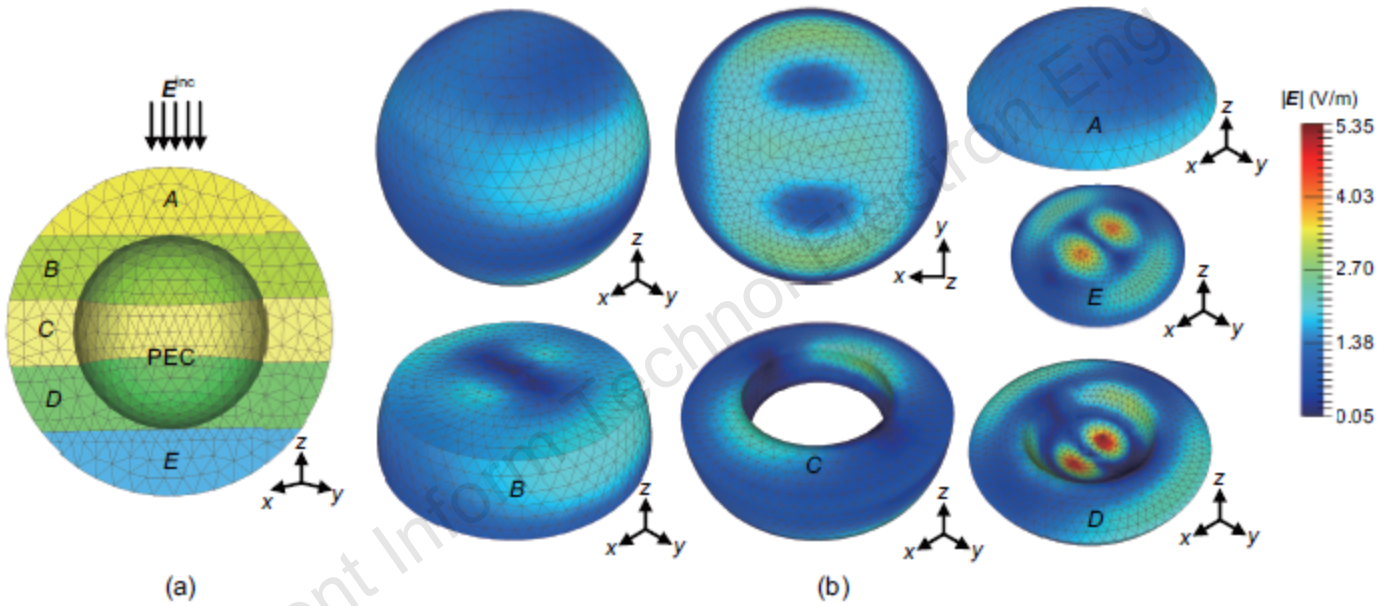

Fig. 5 Model and simulation results of the composite ball

(a) The ball centered at the origin consists of six sub-regions. The inner sphere with a radius of 0.06 m is formed by PEC. The outer layer with a radius of 0.1 m is formed by five dielectric materials A, B, C, D, and E with relative permittivity of 1.5, 2.0, 2.5, 3.0, and 3.5, respectively. The five dielectric sub-regions have the same thickness of 0.04 m. The composite ball is illuminated by a 2.0 GHz vertically polarized incident wave from $(\theta, \phi) = (0°, 0°)$. Note that the concave cut is made for improved visibility. (b) The total field distribution of the object is calculated by the enhanced solution. Different views of the dielectric sub-regions are presented

Major results

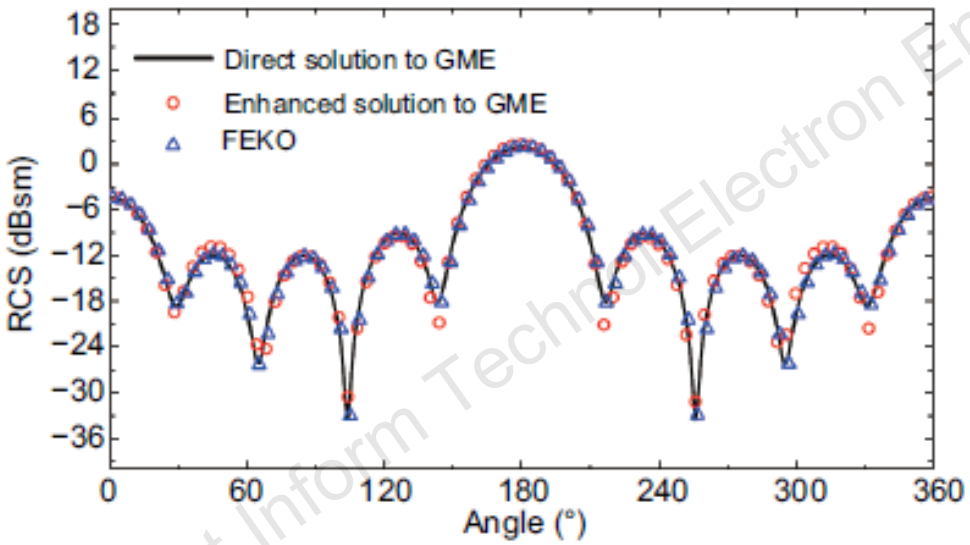

Fig. 6 Bistatic RCS of the composite ball computed by the direct solution, enhanced solution, and FEKO

Major results

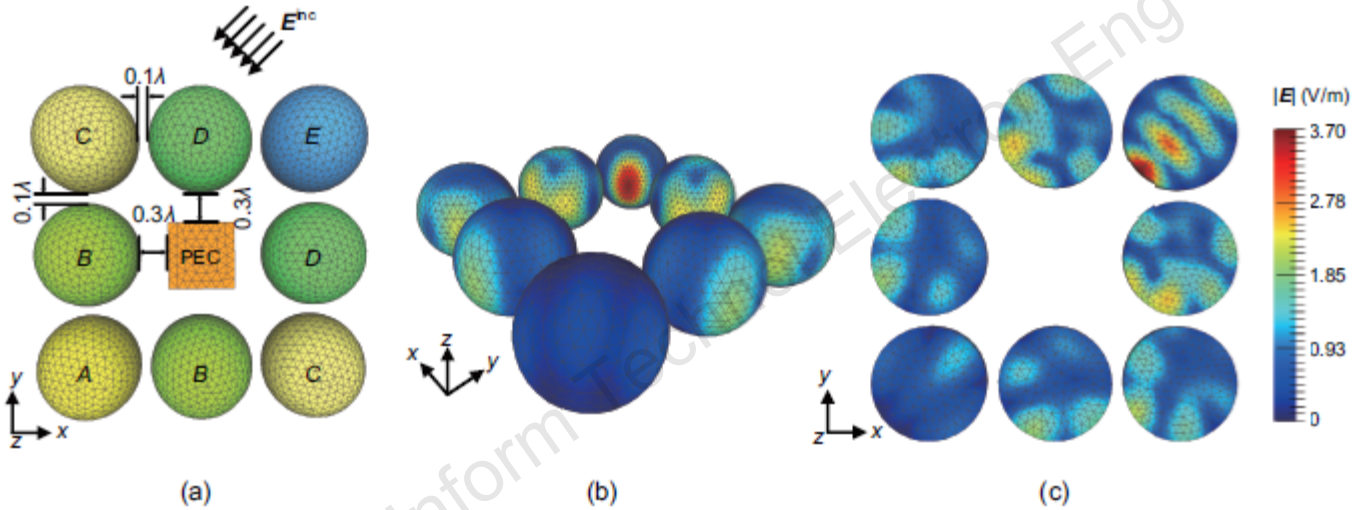

Fig. 7 Model and simulation results of the discrete objects

(a) The discrete objects consist of nine sub-regions. The cube in the center with a side length of 0.06 m is formed by PEC. The eight balls with a radius of 0.05 m around the cube are formed by dielectric materials. The dielectric materials A, B, C, D, and E have relative permittivity of 1.5, 2.0, 2.5, 3.0, and 3.5, respectively. The discrete objects are illuminated by a 3.0 GHz vertically polarized incident wave from $(\theta, \phi) = (90°, 45°)$. (b) The total field distribution among the dielectric sub-regions is calculated by the enhanced solution. (c) The total field distribution among the dielectric regions on the $z = 0$ plane is shown for improved visibility

Major results

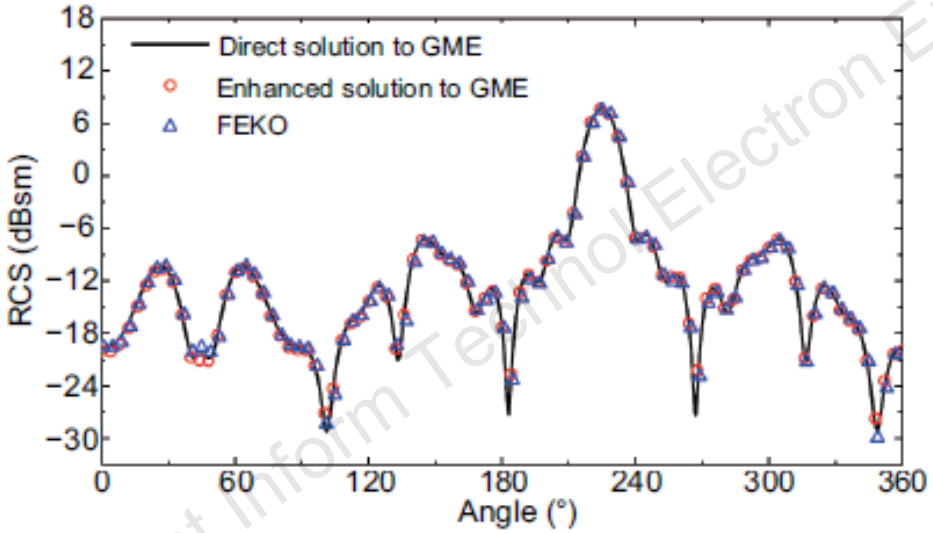

Fig. 8 Bistatic RCS of the discrete object computed by the direct solution, enhanced solution, and FEKO

Conclusions

1. The GME is first presented to analyze arbitrary metal–dielectric composite objects based on SVS-EFIE.

2. Two policies are proposed and can be selected adaptively based on the coupling degree concerning the spacing between different sub-regions.

3. Numerical results demonstrate that the proposed method requires only 11.6% memory and 11.8% CPU time on average compared to the previous direct solution.

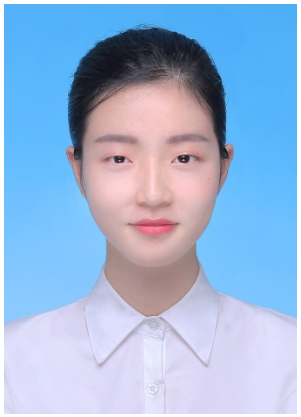

Han WANG received her BS degree in software engineering from Wuhan University, Wuhan, China, in 2019. She is currently pursuing her PhD degree with the College of Computer Science and Technology, Zhejiang University, Hangzhou, China. Her research interests include numerical methods, fast algorithms, and shape optimization.

Mingjie PANG received his BS degree from Zhejiang University, Hangzhou, China, in 2017. He is currently pursuing his PhD degree with the College of Computer Science and Technology, Zhejiang University, Hangzhou, China. His current research interests include computational electromagnetics and wireless channel modeling.

Hai LIN, corresponding author of this paper, received his BS and MS degrees from Xidian University, Xi'an, China, in 1987 and 1990 respectively, and his PhD degree in computer science from Zhejiang University, Hangzhou, China, in 2000. He had been a research fellow in medical visualization at De Montfort University, UK, from 2000 to 2003. He was a visiting professor of the Department of Computing and Information Systems, University of Bedfordshire, UK, from 2013 to 2016. He is currently a professor with the State Key Lab of CAD & CG, Zhejiang University, Hangzhou, China. His current research interests include graphical electromagnetic computing, wireless channel modeling, computer graphics, scientific visualization, and volume rendering.